SCIENCE CHINA
Information Sciences

• **Supplementary File** •

Channel modeling for MI-based wireless underground sensor networks with conductive objects

Shu-Han DENG[1], Guang-Hua LIU[1*], Zi-Wei CHEN[1,2], Huai-Jin ZHANG[1,2] & Tao JIANG[1]

[1]*Research Center of 6G Mobile Communications, School of Cyber Science and Engineering, Huazhong University of Science and Technology, Wuhan* 430074*, China;*
[2]*School of Electronic Information and Communications, Huazhong University of Science and Technology, Wuhan* 430074*, China*

Appendix A Derivation of circuit parameters

As shown in Figure A1, we take the single conductive object equivalent circuit as an example to illustrate the expression of each parameter in the circuit.

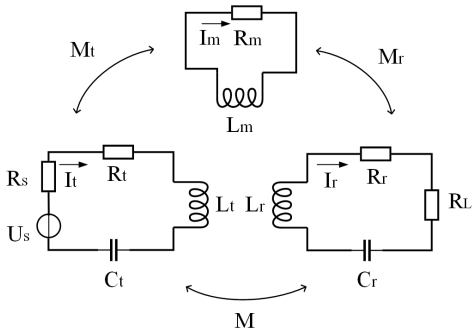

Figure A1 (Color online) Equivalent circuit with one conductive object.

The resistances of the transmitter coil and receiver coil are determined by the material, the size and the number of turns of the coils [1]

$$\begin{aligned} R_{\mathrm{t}} &= 2\pi a_{\mathrm{t}} N_{\mathrm{t}} \rho \\ R_{\mathrm{r}} &= 2\pi a_{\mathrm{r}} N_{\mathrm{r}} \rho, \end{aligned} \tag{A1}$$

where N_{t} and N_{r} are the number of turns of the transmitter and receiver coils, respectively; a_{t} and a_{r} are the radius of the coils; ρ is the resistance per unit length of wire.

The self induction of the transmitter coil and receiver coil can be derived [1]

$$\begin{aligned} L_{\mathrm{t}} &\simeq \frac{1}{2}\mu\pi N_{\mathrm{t}}^2 a_{\mathrm{t}} \\ L_{\mathrm{r}} &\simeq \frac{1}{2}\mu\pi N_{\mathrm{r}}^2 a_{\mathrm{r}}. \end{aligned} \tag{A2}$$

where d is the distance between the coils; respectively; a_{t} and a_{r} are the radius of the transmitter and receiver coils.

In actual MI transmission, we usually need to make the circuits resonant to maximize the power. Hence, we connect the capacitances in series. When the operating frequency is f_0, $\omega_0 = 2\pi f_0$, there is $j\omega_0 L_{\mathrm{t}} + 1/j\omega_0 C_{\mathrm{t}} = j\omega_0 L_{\mathrm{r}} + 1/j\omega_0 C_{\mathrm{r}} = 0$. The capacitances can be expressed by

$$\begin{aligned} C_{\mathrm{t}} &= \frac{1}{\omega_0^2 L_{\mathrm{t}}} \\ C_{\mathrm{r}} &= \frac{1}{\omega_0^2 L_{\mathrm{r}}}. \end{aligned} \tag{A3}$$

* Corresponding author (email: guanghualiu@hust.edu.cn)

For the conductive object, it is assumed that the current is uniformly distributed over the plate thickness and circulates in rectangular paths. The plate is considered as an equivalent LR circuit and its equivalent inductance and resistance are calculated analytically and expressed as a function of the plate dimensions [2].

$$R_m = 4\rho \frac{W^2 + H^2}{lWH} \tag{A4}$$

$$L_m = \frac{2\mu}{3\pi}\left[W\left(1+\ln\frac{W+\sqrt{(W^2+H^2)}}{H}\right)+H\left(1+\ln\frac{H+\sqrt{(W^2+H^2)}}{W}\right)+\frac{W^2-H^2}{\sqrt{(W^2+H^2)}}\ln\frac{H\left(W+\sqrt{(W^2+H^2)}\right)}{W\left(H+\sqrt{(W^2+H^2)}\right)}\right] \tag{A5}$$

where W, H, l are the length, height and thickness of the conductive object. Note that when the skinning depth is greater than the thickness of the metal, the thickness is taken to be the actual thickness of the object, and when the skinning depth is less than the thickness of the metal, the thickness is taken to be the skinning depth.

Appendix B Derivation of shielding factor

The portion of the magnetic field that passes through the metallic medium during propagation undergoes attenuation [3]. We denote the proportion as the shielding factor, and the derivation is as followed.

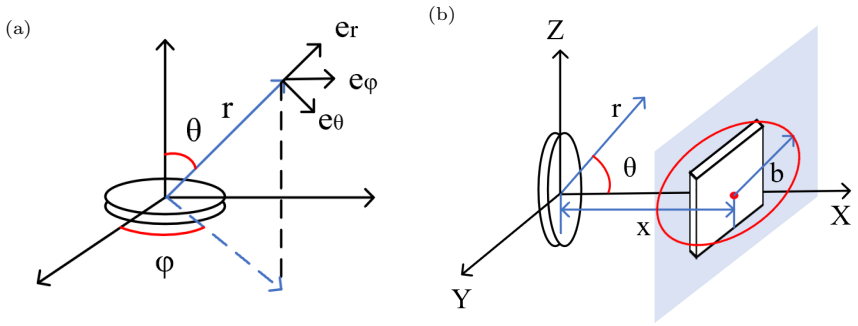

Figure B1 (Color online) Coordinate systems. (a) Spherical coordinate system; (b) rectangular coordinate system.

The spherical coordinate system is established as shown in Figure B1(a). In the near-field range, the magnetic field has properties similar to a static magnetic field, and its magnetic field component can be simplified as [4]

$$\begin{cases} \mathbf{h}_r = \dfrac{2}{4\pi r^3} p_{\mathrm{m}} \cos\theta \mathbf{e}_r \\ \mathbf{h}_\theta = -\dfrac{1}{4\pi r^3} p_{\mathrm{m}} sin\theta \mathbf{e}_\theta \\ \mathbf{h}_\phi = 0, \end{cases} \tag{B1}$$

where $p_{\mathrm{m}} = N \cdot A \cdot I$ is the magnetic dipole moment of the coil; A is the area of the coil; I is the current in the coil. We then set up a right-angled coordinate system based on the actual coil placement, as shown in Figure B1(b). The magnetic field perpendicular to the conductive object is counted as the effective magnetic flux, so only the magnetic field in the x-axis direction is valid. We project the total magnetic field strength onto the x-axis, denoted as

$$\mathbf{h}_x = \frac{p_{\mathrm{m}}}{4\pi r^3}(2\cos\theta^2 - \sin\theta^2)\mathbf{e}_z = \frac{p_m(2x^2 - y^2 - z^2)}{4\pi\left(x^2+y^2+z^2\right)^{2.5}}\mathbf{e}_z. \tag{B2}$$

Assume that the distance of the conductive object from the coil is $x = x_0$. Integrating over $\mathbf{h}_x$ gives the magnetic flux through the conductive object

$$\phi = \int_{\frac{-H}{2}}^{\frac{H}{2}} \int_{\frac{-W}{2}}^{\frac{W}{2}} \frac{\mu_0 p_m (2{x_0}^2 - y^2 - z^2)}{4\pi\left(x_0^2+y^2+z^2\right)^{2.5}} \mathrm{d}y\mathrm{d}z. \tag{B3}$$

We then integrate all magnetic fluxes in the plane where the object is located, as shown in Fig. B1(b).

$$\phi_{\mathrm{total}} \approx \int_0^{\alpha_0} \frac{\mu_0 p_{\mathrm{m}} b(2x_0^2 - b^2)}{2\left(b^2 + {x_0}^2\right)^{2.5}} \mathrm{d}b, \tag{B4}$$

where $b = \sqrt{y^2+z^2}$ is in the plane where the object is located, α_0 is the approximate range of the magnetic field, we take the value of 5 times the radius of the coil, greater than this range can be regarded as a conducting object to infinity [5]. We take the ring of radius b as the integral element. We consider that the magnetic field beyond α_0 is severely attenuated and the magnetic field strength can be negligible at the receiver coil. Therefore, the shielding factor can be expressed as

$$\alpha = \frac{\phi}{\phi_{\mathrm{total}}}. \tag{B5}$$

Note that when the size of the metal plate exceeds 5 times the radius of coil, we have a shielding factor of 1, meaning that any magnetic field that reaches the receiving end is shielded by the metal plate. In this case, the frequency characteristics are no longer the same as they were when partially shielded, and it is progressively more difficult to penetrate the metal plate as the frequency increases [6].

Appendix C Experimental setup and analysis

In this section, we discuss the numerical and experimental results of MI channel with conductive objects. We study the variation of received power with distance, frequency. It is worth noting that in order to simplify the experiment, we conducted the experiment in air instead of in soil. Due to the close magnetic permeability of air and soil, the propagation properties of MI signals in both are almost identical, which does not affect our experimental results.

Experimental setup The system includes a signal generator, resonant circuits, transmitter and receiver coils, and a spectrum analyzer, as shown in Figure C1. The Cartesian coordinate system is established in Figure C2 in order to represent the position of the objects easily. We use copper plates as conductive objects, and the size of the plates is 10 × 10 × 0.05 cm. Specific parameter values in our experiment are shown in Table C1. The parameters used in the simulation are the same as in the experiment. The results data is measured ten times to obtain the average.

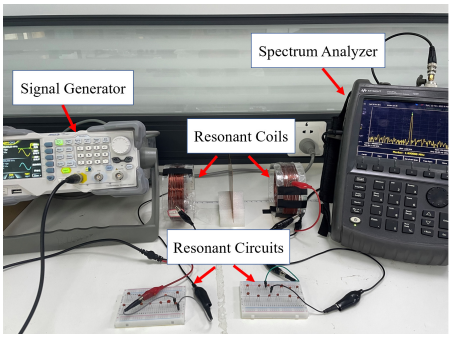

Figure C1 (Color online) Experimental equipment.

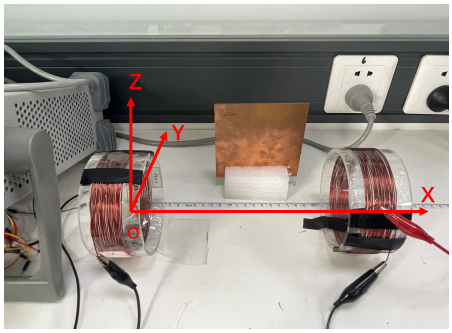

Figure C2 (Color online) Cartesian coordinate system.

Table C1 Experimental parameters

Name of parameter	Value of parameter
Radius of coil	5 cm
Radius of coil wire	0.8 mm
Number of turns of coils	24
Transmitter coil resistance	0.58 Ω
Receiver coil resistance	0.59 Ω
Transmitter coil inductor	86 μH
Receiver coil inductor	86 μH
Supply voltage amplitude	2.5 V
Resistance of power supply	50 Ω
Load resistance	50 Ω
Resistivity of conductive objects	0.0172 Ω· m
Conductivity of conductive objects	47 $\times 10^6$ S/m

The positions of multiple conductive objects are divided into four cases. Multiple reflection: both objects are placed perpendicular to the coil axis with coordinates (5,0.0), (15,0,0); multiple refraction: both objects are placed parallel to the coil axis with coordinates (5,5,0), (15,5,0); mix 1: one object is perpendicular to the axis and one object is parallel to the axis with coordinates (5,0,0), (15,5,0); mix 2: one object is parallel to the axis and one object is perpendicular to the axis with coordinates (5,5,0), (15,0,0). For comparison, we also tested the received power of single conductive object channel, and the coordinates of the conductive object for the reflection case and the refraction case are (5,5,0), (5.0,0), respectively.

Simulation and experimental results First, the received power with different distance is investigated. The distance between the receiver and transmitter coils is from 0.2 m to 0.5 m. The position of the transmitter coil remains constant and the receiver coil is gradually moved away. The operating frequency is 0.82 MHz, and we make the transceiver circuit resonate at the operating frequency by adjusting the resonant capacitor before adding the metal.

Figure C3(a) and C3(b) shows the received power of original channel, single reflection channel and single refraction channel. The variation trend in the experiment is similar to that in the simulation. The change in distance resulted in a 22.9 dBm decrease in received power in the experiment and an 18.6 dBm decrease in the simulation. It can be observed that reflection enhances the received power while refraction reduces it. Specifically, the received power of the reflection channel increases by an average of 0.36 dBm while the power of the refraction channel decreases by an average of 1.24 dBm in the experiment, compared to the original channel. In the simulation, the power of the reflection channel increases by an average of 0.2 dBm while the power of the refraction channel decreases by an average of 0.92 dBm. In addition, as shown in Figure C3(c) and C3(d), multiple reflection channel further improves the received power, with an average increase of 0.57 dBm compared to the single reflection channel in the experiment. And the multiple refraction channel reduces the power by an average of 2 dBm compared to the single refraction channel. In the simulation, the multiple reflection channel causes an additional 0.23 dBm power gain and multiple refraction channel caused an additional 1.9 dBm power loss. What's more, compared to the single refraction, Mix 1 has a slight increase in received power due to an additional reflection object compared to the single refraction channel, while Mix 2 has a lower received power due to the additional effect of refraction object compared to the single reflection channel. This shows that the influence of multiple conductive objects acts as a superposition of individual objects.

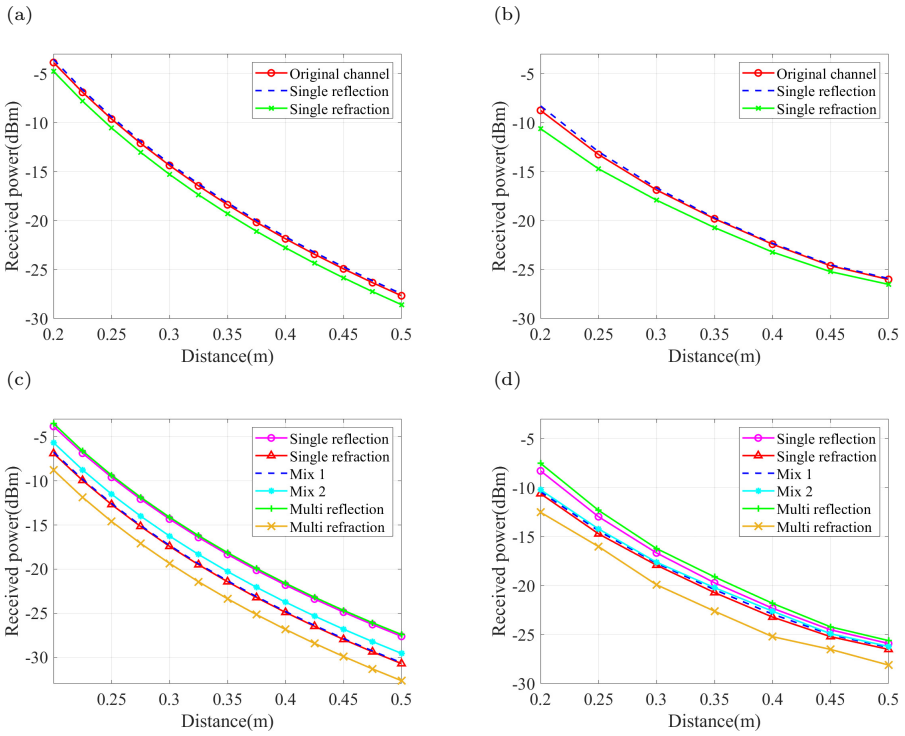

Figure C3 (Color online) Received power at different distances. (a) Calculated data: one single conductors; (b) experimental data: one single conductors; (c) calculated data: multiple conductors; (d) experimental data: multiple conductors.

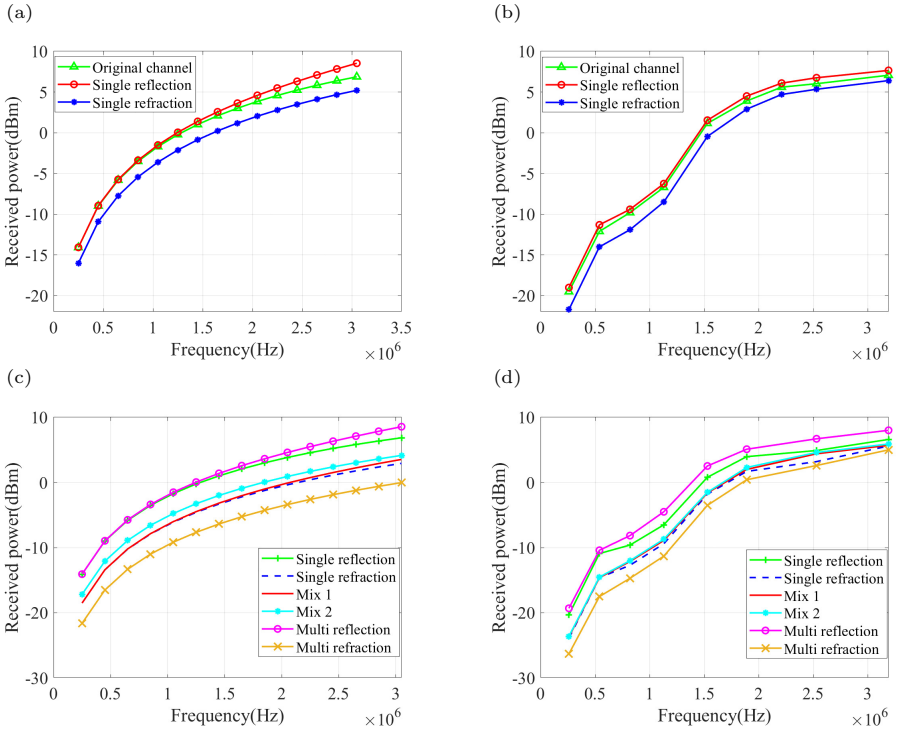

Figure C4 (Color online) Received power at different frequencies. (a) Calculated data: one single conductors; (b) experimental data: one single conductors; (c) calculated data: multiple conductors; (d) experimental data: multiple conductors.

Next, the MI channel with conductive objects at different frequencies is studied. The frequency domain characteristics of the channel are of vital importance since the operating frequency is not fixed in the actual MI communication [7]. The frequency changes from 0.25 MHz to 3.2 MHz and each frequency has its own corresponding capacitance in order to resonate the receiver and transmitter circuits. The distance between the coils is fixed at 20 cm.

As shown in Figure C4, the experimental result shows a good match with the theoretical calculation. It can be found that the

received power increases with the increase of frequency in all cases. The change in frequency resulted in a 26.5 dBm increase in received power in the experiment and an 22.3 dBm increase in the simulation. Figure C4(a) and C4(b) illustrate the received power of a single conductor. In the experiment, an average gain of 0.55 dBm is obtained by reflection and an average attenuation of 1.53 dBm is obtained by refraction compared to the channel without conductive objects. In the simulation, an average gain of 0.61 dBm is obtained by reflection and an average attenuation of 1.83 dBm is obtained by refraction. Figure C4(c) and C4(d) illustrate the received power of multiple conductors. In the experiments, the multiple reflection channel increases the received power by an average of 0.96 dBm over the single reflection channel, and the multiple refraction channel reduces the loss by an average of 2.1 dBm over the single refraction channel. In the simulation, the multiple refraction channel gains an additional 1.18 dBm of power and the the multiple refraction channel loses an additional 1.78 dBm of power. For Mix 1 and Mix 2, the received power is between single refraction and single reflection.

Discussion From the results above, the average percentage error between the results of the channel model and the measured data is 39%, where half of the frequency points can have an error of 14% or less. Our model can relatively accurately portray the actual channel. The experimental data are relatively smaller, which is due to the circuit losses and the Joule heat consumed by the metal plate. We can draw the following conclusions from the comparison of experimental and simulation results. First, the MI channel has a frequency-selective property and higher frequency is more favorable for signal transmission [8]. In more details, as the frequency increases, the enhancement of the signal by refraction object gradually increases. Additionally, refraction objects has greater influence on received power than that of reflection objects. And the influence of multiple conductive objects acts as a superposition of individual objects: the received power of multiple refraction suffers greater attenuation, the received power of multiple reflection suffers greater increase, and in mix channel, the power is a compromise between the single reflection and single refraction. What's more, the placement of the conductive objects also affects received power. When the reflection object is closer to the transmitter coil and the refraction object is farther away (in Mix 2), the received power is slightly greater than the situation when the positions are swapped (in Mix 1). This is due to the relatively high magnetic induction strength near the transmitter coil, which causes greater density of eddy currents in conductive objects. Our proposed channel model is only an exploratory work, improving the accuracy of the model and verifying the model in more realistic scenario, like underground mines that include metallic minerals will be our subsequent work.

References

1 Sun Z, Akyildiz I F. Magnetic induction communications for wireless underground sensor networks. IEEE Transactions on Antennas and Propagation, 2010, 58: 2426-2435

2 Siakavellas N J. Analytical modelling of eddy currents induced by a time-varying magnetic field in a conductive plate. The international journal for computation and mathematics in electrical and electronic engineering, 1994, 13(3): 497-508.

3 Kisseleff, S, Akyildiz I F, and Gerstacker W H. Digital signal transmission in magnetic induction based wireless underground sensor networks. IEEE Transactions on Communications, 2015, 63(6): 2300-2311.

4 Morag Y, Tal N, Leviatan Y, et al. "Channel capacity of magnetic communication in a general medium incorporating full-wave analysis and high-frequency effects." IEEE Transactions on Antennas and Propagation, 2019, 67(6): 4104-4118.

5 Huang R C, Lu M Y, Peyton A, et al. Thickness measurement of metallic plates with finite planar dimension using eddy current method. IEEE Transactions on Instrumentation and Measurement, 2020, 69(10): 8424-8431.

6 Qin D Yu, and Jiao C Q. Low-frequency magnetic shielding of planar screens: Effects of loop radius and loop-to-loop distance. IEEE Transactions on Electromagnetic Compatibility 2021, 64(2): 367-377.

7 Liu G H. A q-learning-based distributed routing protocol for frequency-switchable magnetic induction-based wireless underground sensor networks. Future Generation Computer Systems, 2023, 139: 253-266

8 Tan X, Sun Z, and Akyildiz I F. Wireless underground sensor networks: MI-based communication systems for underground applications. IEEE Antennas and Propagation Magazine, 2015, 57(4): 74-87.